Towards trapping of molecular ions in a linear Paul Trap

Emil Lenler-Eriksen

PhD Progress Report

Abstract

An abstract...

Contents

Introduction

In the 1950's Wolfgang Paul invented the so-called Paul trap, for trapping charged particles within a quadrupolar electromagnetic field.CITE. In 1989 he would go on to recieve the Nobel Prize in physics, alongside Hans Dehmelt, "for the development of the ion trap technique" CITE. With the many technological and scientific advancements since the Paul trap's inception, among which the laser is an especially important one, it is now possible to trap, and cool single ions to temperatures below 1mK CITE Wineland. Such cold ions pose many interesting possibilities for science, as they can make good candidates for atomic clocks CLOCK, or the basis for quantum computers Wineland, Cirac Zoller.

Paul traps are also used for the study of fluorescence of molecules in the gas phase CITE Steen?, where pulsed lasers can be used to excite large clouds of molecular ions, whose fluorescence spectrum may then be recorded and studied. However as most molecules lack the necessary energy level structure for laser cooling, the temperature of these experiments are limited by their cryogenic cooling environment.

The aim of my PhD thesis is to build an experiment where single molecular ions from an electrospray ionization source FENN can be trapped in a linear Paul trap alongside a Ba^+ ion and cooled to their motional ground state. In such a setup we would like to investigate the molecules using a method called photon recoil spectroscopy CITE EMILIE. This method functions by using the momentum kick associated with the molecules absorption of light as a measure of whether absorption has occured, and is explained further in chapter 5. Directly applying this method to two-ion systems with large mismatches in mass and charge is challenging, since the motions of the ions are only very weakly coupled, and thus the absorption kick will predominantly excite the motion of the molecule, which is not sensitive to the readout performed by a laser on the Ba^+ ion. Due to this issue I have been looking at CITE, and developing theory for how to transfer energy from one motional mode to another, to allow for efficient readout of the absorption kick.

Outline of the report

The report is divided into 6 different chapters. Chapter 1 is a brief introduction to the field, some of the challenges I face, and what I hope to accomplish with my PhD.

Chapter 2 describes the physics of trapping ions in a linear Paul trap and is split into two sections, the first describing the trapping of a single ion, while the latter derives the common motion of two ions in the trap.

Next is chapter 3 which describes the electrospray ionization source, which is the source of molecular ions for the experiment. The first section of this chapter is an overview of the setup and the second contains a characterization of one of the octopoles guides within the setup.

After that I move on to chapter 4 which describes the laser cooling necessary for eventually reaching the motional ground state of a two-ion system. The first section contains the theory for doppler cooling, which allows the ions to reach a temperature of ~1mK. The second section describes sideband cooling, which is necessary to cool the motion of the system to its quantum mechanical ground state. Finally the 3rd section of this chapter talks on how one can couple the motion of the ions by using fx. an external field, in order to improve the cooling of systems where the two ions have large differences in mass and charge.

Finally chapter 6 gives a short plan of the work I plan to do in the latter half of my PhD studies here at Aarhus.

The Linear Paul Trap

2.1 Single ion in a linear Paul Trap

The linear Paul trap consists of four rods, each of which is split into three electrodes as is seen on fig. 2.1. The coordinate system for the trap is defined such that the z-axis runs down along the centre of the trap, while the x, y-axes go between diagonally opposed rods. Furthermore we define z_0 to be half the length of center electrodes, while we define r_0 as half the distance between diagoanlly opposed electrodes as seen on fig. 2.1. In order to trap an ion along the z-direction a static voltage V_{end} is applied to all of the electrodes on the end of the rods. By applying such a votlage to these endcap electrodes an electrical potential is generated, which in the region around the centre of the trap can be written as

$$\phi_{DC}(z) = \frac{\kappa V_{end}}{z_0^2} z^2, \tag{2.1}$$

where κ is a constant defined by the specific geometry of the trap, and z is the position of the ion along the z axis. Thus an ion of mass m and charge Q finds itself sitting in a harmonic potential

$$V_{DC}(z) = \frac{1}{2} m \omega_z^2 z^2, \quad \omega_z = \sqrt{\frac{2Q\kappa V_{end}}{mz_0^2}}, \tag{2.2}$$
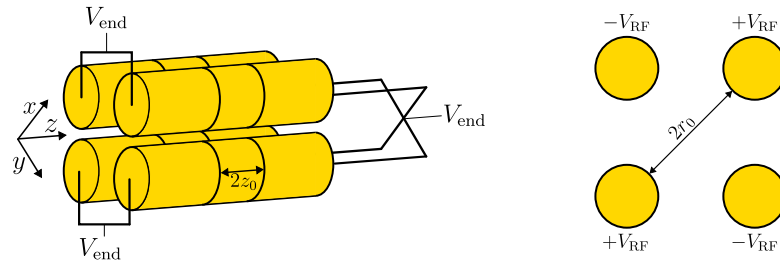

FIGURE 2.1: Example schematic of a linear paul trap showing: (left) a 3D model of the paul Trap with both the DC endcap voltages applied. (right) an end-view down the Paul trap, showing the phase of the RF voltages applied to the different rods..

where ω_z is the frequency of the ions oscillating motion along the z-axis.

For the radial directions it is necessary to take a slightly different approach, indeed Earnshaw's theorem Earnshaw states that it is impossible to trap a charged particle in all three directions, solely through the use of electrostatic forces. If we look at the electrical potential in the x, y-plane from the DC endcaps we also find

$$\phi_{DC}(x, y) = -\frac{\kappa V_{end}}{2z_0^2}(x^2 + y^2),\tag{2.3}$$

which is clearly repulsing the ion from the center of the trap.

To counteract this repulsive effect, we employ an RF voltage, oscillating at frequency Ω_{RF}, with an amplitude V_{RF} on all four rods. Neighbouring rods have opposites phases while, dioganlly opposing rods share a phase, as seen on fig. 2.1. We can then write the total time dependant electrical potential in the x, y-plane as
KARIN

$$\phi(x, y, t) = -\frac{\kappa V_{end}}{2z_0^2}(x^2 + y^2) - \frac{V_{RF}}{2r_0^2}(x^2 - y^2)\cos(\Omega_{RF}t),\tag{2.4}$$

where the first term comes from the repulsing DC potential, and the second term comes from the RF voltages applied to the rods.

The equations of motion in the radial plane can be rewritten on a more compact form by adopting the notation

$$\tau = \frac{\Omega_{RF}t}{2}, \quad a = -\frac{4Q\kappa V_{DC}}{mz_0^2\Omega_{RF}^2}, \quad q_x = -q_y = \frac{2QV_{RF}}{mr_0^2\Omega_{RF}^2},\tag{2.5}$$

which allows for the equations of motion to be written as

$$\frac{d^2\gamma}{d\tau^2} + (a - 2q_\gamma\cos(2\tau))\gamma, \quad \gamma \in \{x, y\}.\tag{2.6}$$

Equation (2.6) is known as the Mathieu equation CITE, the Mathieu equation has bounded solutions for several sets of (a, q_γ) parameters, however, the conditions usually used in experiment state that for a given value of q_γ, a must be found between the two curves approximated by CITE

$$a_0(q_\gamma) \approx -\frac{1}{2}q_\gamma^2 + \frac{7}{128}q_\gamma^4 - \frac{29}{2304}q_\gamma^6 + \frac{68687}{18874368}q_\gamma^8,\tag{2.7}$$

$$b_1(q_\gamma) \approx 1 - q_\gamma - \frac{1}{8}q_\gamma^2 + \frac{1}{64}q_\gamma^3 - \frac{1}{1536}q_\gamma^4 - \frac{11}{36864}q_\gamma^5.\tag{2.8}$$

Together these two lines form what is known as a stability diagram. Since a positive DC voltage is needed for the confinement in the axial direction, we usually confine ourselves to considering stability in the $a < 0$ region. A plot of the stable region for the linear Paul trap can be see on fig. 2.2

In the case where $|a|, |q_\gamma| \ll 1$ the solution to eq. (2.6) can be approximated to

$$\gamma(t) = \gamma_0\left(1 - \frac{q_\gamma}{2}\cos(\Omega_{RF}t)\right)\cos(\omega_r t), \quad \omega_r = \frac{\Omega_{RF}}{2}\sqrt{\frac{q_\gamma^2}{2} + a}.\tag{2.9}$$

Since $|q_\gamma| \ll 1$ we see that there is a large-amplitude motion of the ion at frequency ω_r. This motion is typically referred to as secular motion in the litterature. The
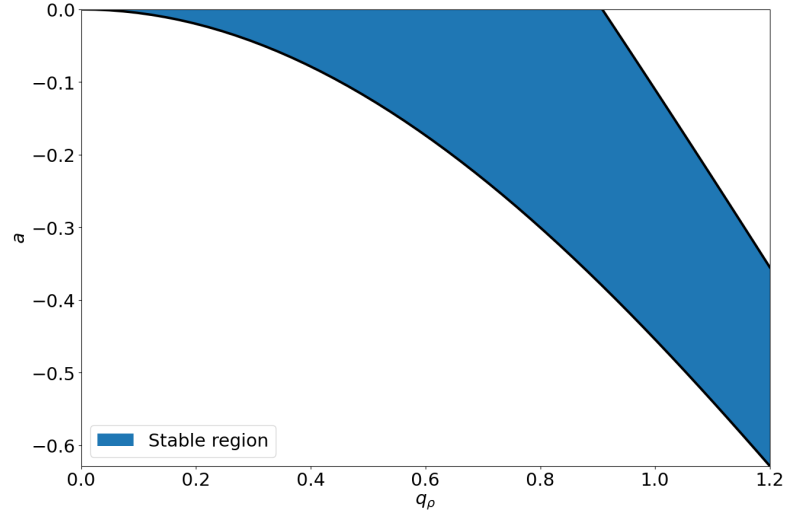
FIGURE 2.2: Plot of the Mathieu stability diagram for negative values of a. The blue colored area contains the set of bounded, and thus stable solution to the Mathieu equation of eq. (2.6).
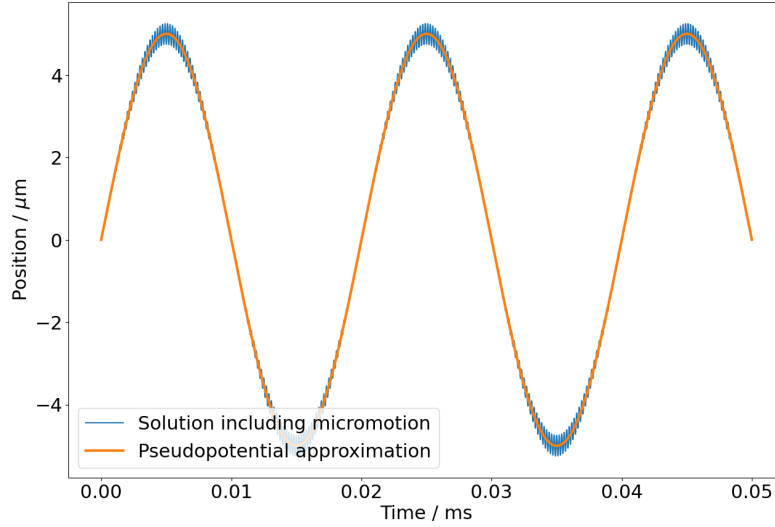

FIGURE 2.3: Trajectories including (blue) micromotion or calculated through the pseudopotential approximation (orange), for $\gamma_0 = 5\mu$m, $\omega_r = 2\pi \times 50$kHz, $\Omega_{RF} = 2\pi \times 5.2$MHz..

frequency ω_r is much slower than the RF frequency of the trap (typically 10's-100's of kHz vs. 5MHz in the case of our trap).

In addition there is a small-amplitude motion superimposed on top, oscillating at the RF frequency. This motion is typically referred to as micromotion. Thus the full picture we now get, is one of the ion performing slow, but large oscillations in the radial plane, with an additional micromotion on top. An example trajectory can be seen on fig. 2.3, where the micromotion is clearly visible.

It is common to average over the micromotion of the ion, keeping only the term oscillating at ω_r. If this is done, it is clear that the ion then moves as if in an effective

potential (often referred to as pseudopotential in the litterature) given by

$$V_{Pseudo}(\gamma) = \frac{1}{2}m\omega_r^2\gamma^2, \quad \gamma \in \{x, y\}. \tag{2.10}$$

The pseudopotential approximation is especially useful when working with trapped ions in a quantum mechanical regime, since their Hamiltonian is then simply that of a harmonic oscillator, which is one of the most well-studied examples in all of quantum mechanics.

2.2   Two ions in a linear Paul trap

We now move on to the topic of two co-trapped ions in a Paul trap. We shall denote the ions 1 and 2 respectively, with masses m_1, m_2, and charges Q_1, Q_2. Remembering to include the Coulomb interaction between the two ions, the potential energy of the system, in the pseudopotential approximation, can then be written as

$$V(\mathbf{r_1}, \mathbf{r_2}) = \frac{1}{2}m_1\left(\omega_{1,z}^2 z_1^2 + \omega_{1,r}^2(x_1^2 + y_1^2)\right) + \frac{1}{2}m_2\left(\omega_{2,z}^2 + \omega_{2,r}^2(x_2^2 + y_2^2)\right)$$
$$+ \frac{Q_2 Q_2}{4\pi\epsilon_0}\frac{1}{|r_1 - r_2|}, \tag{2.11}$$

where $\omega_{j,(r/z)}$ is calculated as in eqs. (2.2) and (2.9), using the mass and charge of ion j. For the rest of the derivations in this report we are, unless otherwise noted, going to ignore the y part of motion of the ions since our system exhibits a radial symmetry, and thus any equations that hold for x will hold for y as well.

We shall first derive the equilibrium positions for the two ions. Assuming the radial trapping is stronger than the axial trapping we know that the ions will along themselves along the z-axis, and thus we slightly simplify the potential to be minimized

$$V(z_1, z_2) = \frac{1}{2}m_1\omega_{1,z}^2 z_1^2 + \frac{1}{2}m_2\omega_{2,z}^2 z_2^2 + \frac{Q_1 Q_2}{4\pi\epsilon_0}\frac{1}{z_1 - z_2}, \tag{2.12}$$

where we assume without loss of generality that $z_1 > z_2$. Taking the derivatives with respect to the ion coordinates to be zero we find

$$\frac{\partial V}{\partial z_1} = m_1\omega_{1,z}^2 z_{1,eq} - \frac{Q_1 Q_2}{4\pi\epsilon_0}\frac{1}{(z_{1,eq} - z_{2,eq})^2} = 0, \tag{2.13}$$

$$\frac{\partial V}{\partial z_2} = m_2\omega_{2,z}^2 z_{2,eq} + \frac{Q_1 Q_2}{4\pi\epsilon_0}\frac{1}{(z_{1,eq} - z_{2,eq})^2} = 0, \tag{2.14}$$

where the (eq) subscript denotes the value is taken at the equilibrium position. Adding the two together we find

$$z_{1,eq} = -\rho z_{2,eq}, \tag{2.15}$$

where $\rho = \frac{Q_2}{Q_1}$ is the charge ratio between the two ions. It is interesting to note that the equilibrium positions are entirely independent on the masses of the ions. We can now plug this relationship back into eq. (2.13) to find an expression for $z_{1,eq}$

$$z_{1,eq} = \left(\frac{Q_1 Q_2}{4\pi\epsilon_0 m_1\omega_{1,z}^2}\frac{1}{(1 + \frac{1}{\rho})^2}\right)^{1/3}, \tag{2.16}$$
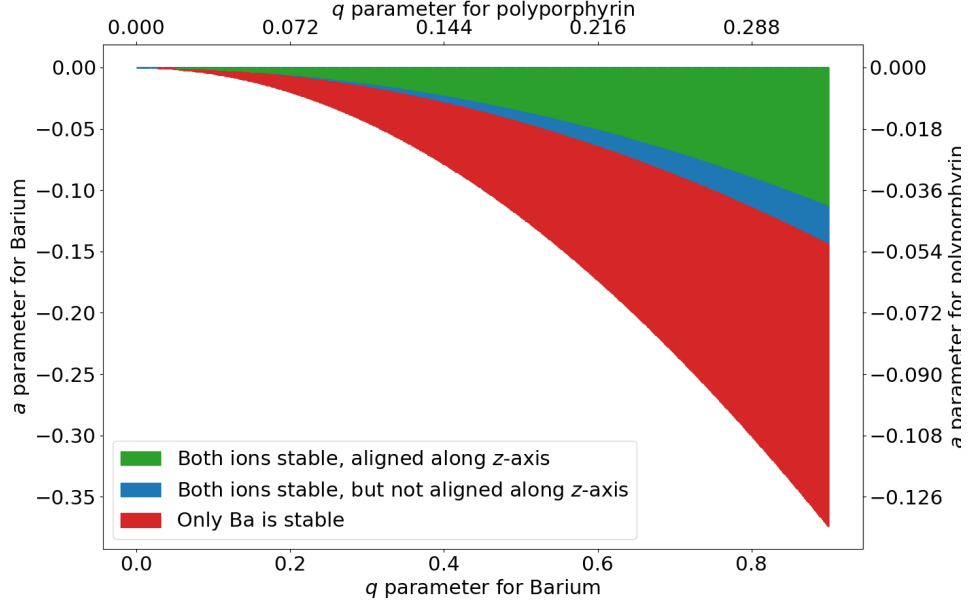
FIGURE 2.4: Stability diagram for Ba^+ cotrapped alongside a polyporphyrin system, holding 12 porphyrin rings with 2 charges each for a total of $m_2 = 9000$amu, $Q_2 = 24e$. The green area represents the a and q parameters ideal for experiments as both ions have stable trajectories, while they also align along the z-axis. for trapping parameters that fall within the blue area the ions have stable trajectories, but will aliugn along the radial axes. Finally the red shaded area describes the parameters for which only the Ba^+ ion has stable trajectories. It is thus clear that trapping two ions with very different mass-to-charge ratios puts considerable additional bounds on the stability of the system..

it has to be noted that if one expands the $\omega_{1,z}$ factor in the denominator one finds that the equilibrium position is mass independent. This has not been done here, as it lengthens the expression considerably.

In this derivation we assumed that the ions aligned themselves along the z-axis, which is also the desired case. However one of course has to design any experiment such that the voltages applied result in such an orientation. This leads to further "stability" requirements for the two-ion system. Following the derivation above one can similarly find expressions for equilibrium positions along the x-axis. The ions will naturally align themselves along the axis which has the lowest energy at equilibrium. Through much massaging, one finds, that if the ions are to align along z, the follow inequality must hold:

$$\frac{m_1 m_2 \omega_{1,z}^2 \omega_{2,z}^2}{m_1 \omega_{1,z}^2 + m_2 \omega_{2,z}^2} < \frac{m_1 m_2 \omega_{1,r}^2 \omega_{2,r}^2}{m_1 \omega_{1,r}^2 + m_2 \omega_{2,r}^2}. \tag{2.17}$$

In addition to this, the ions must also uphold the stability criterium outlined in section 2.1. Given that both ions need to be stable *and* trapped along the z-axis the new stability diagram can look considerably different. An example for a polyporphyrin of mass 9000amu and charge 24e trapped alongside Ba^+ is seen on fig. 2.4.

With the equilibrium positions of the ions, and the criteria for them to be stably trapped determined. One can now determine the new oscillation frequencies of the ions. To do this we reintroduce the full potential of eq. (2.11) and perform a Taylor expansion to 2nd order around the equilibrium position of the system. When performing calculations of vibrational modes for coupled oscillators it is common to introduce mass-weighted displacement coordinates defined as

$$\xi_1 = \sqrt{m_1}(z_{eq,1} - z_1), \quad \xi_2 = \sqrt{m_2}(z_{2,eq} - z_2), \quad \xi_3 = \sqrt{m_1}x_1, \quad \xi_4 = \sqrt{m_2}x_2. \quad (2.18)$$

If we write up the Lagrangian this coordinate system, we find

$$\mathcal{L} = \sum_{i=1}^{4} \dot{\xi}_i^2 - \frac{1}{2} \sum_{i=1}^{4} K_{ij}\xi_i\xi_j, \qquad (2.19)$$

where $K_{ij} = \left(\left.\frac{\partial^2 V}{\partial r_i \partial r_j}\right|_{eq} / \sqrt{m_i m_j} \right)$ and $\{r_1, r_2, r_3, r_4\} = \{z_1, z_2, x_1, x_2\}$. It should be noted that the Taylor expansion in principle also adds an energy offset corresponding to the potential energy when the system is in equilibrium. We ignore this offset as it introduces no dynamics.

Explicit calculation of the K_{ij} terms grants several zero's. The non-zero K_{ij}'s evaluate to

$$K_{11} = \omega_{1,z}^2 \left(1 + \frac{2}{1 + 1/\rho} \right), \qquad (2.20)$$

$$K_{12} = K_{21} = -\frac{2\omega_{1,z}^2}{\sqrt{\mu}(1 + 1/\rho)}, \qquad (2.21)$$

$$K_{22} = \omega_{1,z}^2 \frac{\rho}{\mu} \left(1 + \frac{2}{1 + \rho} \right), \qquad (2.22)$$

$$K_{33} = \omega_{1,r}^2 - \frac{\omega_{1,z}^2}{1 + 1/\rho}, \qquad (2.23)$$

$$K_{34} = K_{43} = -\frac{1}{2}K_{12}, \qquad (2.24)$$

$$K_{44} = \omega_{2,r}^2 - \frac{\omega_{1,z}^2}{\mu(1 + 1/\rho)}. \qquad (2.25)$$

The coupled motional modes as well as their oscillation frequencies can now be found by diagonalizing the matrix TAYLOR

$$K = \begin{bmatrix} K_{11} & K_{12} & 0 & 0 \\ K_{21} & K_{22} & 0 & 0 \\ 0 & 0 & K_{33} & K_{34} \\ 0 & 0 & K_{43} & K_{44} \end{bmatrix}, \qquad (2.26)$$

which is block diagonal. This simplifies the problem significantly, as it suffices to solve the eigenproblem for the two 2x2 matrices on the diagonal

$$K_z = \begin{bmatrix} K_{11} & K_{12} \\ K_{21} & K_{22} \end{bmatrix}, \quad K_r \begin{bmatrix} K_{33} & K_{34} \\ K_{43} & K_{44} \end{bmatrix}, \qquad (2.27)$$

which will give the solutions for the axial and radial motion respectively. Solving the probem yields two modes for each direction, one where the ions move together in-phase with one another (sometimes referred to as the center-of-mass mode), and one where they move out of phase (sometimes referred to as the breathing mode). For the frequencies one finds

$$\left(\omega_z^{i/o}\right)^2 = \frac{K_{11} + K_{22} \mp \sqrt{(K_{11} - K_{22})^2 + 4K_{12}^2}}{2}, \tag{2.28}$$

$$\left(\omega_r^{i/o}\right)^2 = \frac{K_{33} + K_{44} \pm \sqrt{(K_{33} - K_{44})^2 + 4K_{34}^2}}{2}. \tag{2.29}$$

Expanding the K_{ij}'s above would make the equations considerably harder to read, and as such is not done here. Denoting the normalized eigenmodes for the axial motion as $\boldsymbol{\alpha}_{i/o}$, and the ones for radial motion $\boldsymbol{\beta}_{i/o}$ one finds

$$\boldsymbol{\alpha}_{i/o} = \frac{1}{\sqrt{1 + \tilde{\alpha}_{i/o}^2}} \begin{pmatrix} \tilde{\alpha}_{i/o} \\ 1 \end{pmatrix}, \quad \tilde{\alpha}_{i/o} = \frac{\left(\omega_z^{i/o}\right)^2 - K_{22}}{K_{12}}, \tag{2.30}$$

$$\boldsymbol{\beta}_{i/o} = \frac{1}{\sqrt{1 + \tilde{\beta}_{i/o}^2}} \begin{pmatrix} \tilde{\beta}_{i/o} \\ 1 \end{pmatrix}, \quad \tilde{\beta}_{i/o} = \frac{\left(\omega_r^{i/o}\right)^2 - K_{44}}{K_{34}}. \tag{2.31}$$

Here the first component of the vector describes the amplitude, often referred to as the contribution or participation, of ion 1 in the motional mode, while the 2nd component of the vector describes the participation of ion 2.

For ions with very different charge-to-mass ratios one finds that the motion of the ions becomes essentially uncoupled. As an example we consider once again a Ba$^+$ ion trapped alongside a polyporphyrin ($m_2 = 9000$amu, $Q_2 = 24$e), here the axial eigenvector for the in-phase motion is $\boldsymbol{\alpha}_i = (0.092, 0.99)$. Thus the in-phase motion of this system consists of almost exclusively motion of the heavy polyporphyrin. This decoupling of motion has significant consequences for cooling, as will be seen in chapter 4.

Further expansion of the equations above makes them considerably harder to read, and thus is not done here. However, it is good to note that, roughly, one finds that $\tilde{\alpha}_{i/o} \propto \rho/\mu$, while $\tilde{\beta}_{i/o} \propto (\rho/\mu)^2$. This means the decoupling of the ion motion tends to be larger along the radial direction as the charge and mass ratios of the two ions become more skewed. ADD INFO ABOUT PAPER WITH MATTEO

Electrospray ionization source

3.1 Overview of the electrospray and its components

As the source of molecular ions for the experiment we implement a so-called electrospray ionization (ESI) source FENN,STEEN. The ESI source we use can be seen connected to the rest of the experiment on fig. 3.1. The basics of how such a device functions is that it has a syringe containing a solvent (typically methanol) with the ions or molecules one wishes to perform experiments on. The syringe is connected to a needle, and a motor slowly depresses the plunger on the syring, causing the solvent to form a droplet on the tip of the needle. The needletip of the ESI source is sitting outside the vaccuum chambers of the ESI setup, in atmospheric air as can be seen on fig.. Opposite of the needle is a narrow opening into the full body of the ESI source, which is put at a very large voltage difference to the tip of the needle (typically 3-3.5kV), this voltage difference leads to a strong electric field which will drag ion
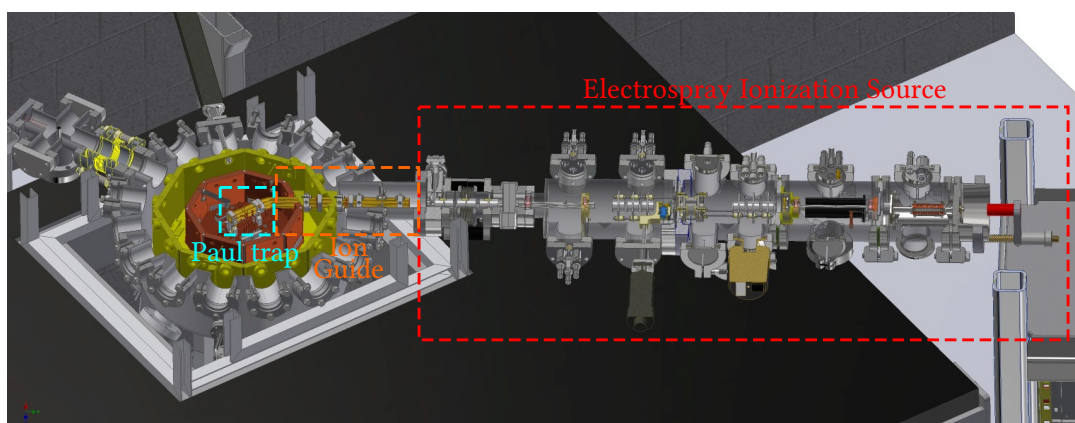

FIGURE 3.1: 3D figure of the full setup at Aarhus, when the electrospray (red) is conneacted to the cryogenic trap. The ion guide (orange) allows to transfer the ions into the cryogenic Paul trap (blue), where experiments will be conducted. At the time of writing the ESI source is not hooked up to the experiment, and instead there is channeltron detector at the very end of the electrospray, where it would connect to the ion guide..
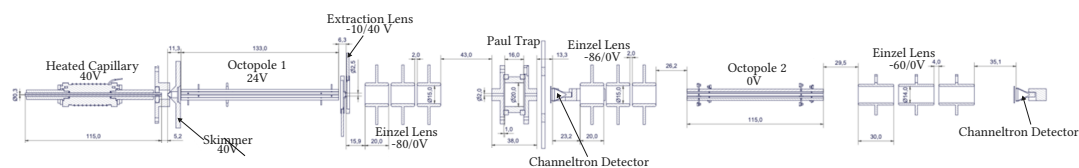
FIGURE 3.2: Technical drawing giving a sideview of all the components of the ESI source we employ. Some of the most important components on the figure have been labelled by name and the voltages typically emplyed on them. It is very important to ensure that there is a voltage gradient as one progresses down the ESI source, since otherwise the ions cannot travel. The multiple voltages noted for the Einzel lenses correspond to outer/inner electrode voltages, and for the extraction lens, the low voltage is set for extraction, while the high is for accumulation..
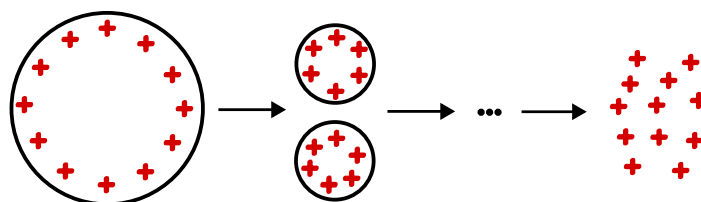

FIGURE 3.3: Illustration of the evaporation principle that allows for gas-phase ions in electrospraying. As the solvent evaporates, the droplet will shrink, until the surface tension becomes unable to counteract the electrostatic repulsion of the ions. This splits the droplet into two droplets, for which this process then repeats. Eventually all the solvent is evaporated and only gas-phase ions are left. Note that the number of ions within a droplet has been grossly underestimated for ease of illustration.

droplets from the needle and into the narrow opening of the ionization source. The ions then enter a capillary tube (see fig. 3.2) heated to 70 degrees celsius, which is set at some voltage (typically 40V). Within the heated cappillary the solvent will begin to evaporate, causing the droplets to shrink. This causes the Coulomb repulsion of the ions within the droplet to increase as they all move nearer. Eventually the surface tension of the droplet can no longer compensate the electrostatic repulsion of the ions within, and the droplet splits. This process repeats until all the solvent is evaporated and the ions are situated in the gas-phase. A schematic of this principle is illustrated on fig. 3.3.

After the evaporation process, gas-phase ions travel past a skimmer and into an octopole storage device. The octopole allows for efficient transport of the ions across long regions, as well as a source of buffer gas cooling to room temperature, due to ion-neutral collisions with the atmospheric gas at a pressure of approx 1mbar. At the very end of the octopole is a pair of "extraction" lenses. We have timed control of these electrodes, allowing us to set them to bunch electrodes in the octopole by setting a high voltage on them, and then releasing the ion bunch by lowering the voltage. I have performed several experiments on this part of the trap, to characterize the storage capabilities of the octopole, as well as the form of the ion bunches that arrive from it. The results of those investigations are found in section 3.2.

Upon extraction from the octopole the ions pass through an Einzel lens. This is a set of three electrodes, where the outer two share the same voltage, and fulfills the same role for ions as a lens does for optics. We use the Einzel lens to focus down the ion beam onto the 2mm wide opening of a cylindrical Paul trap.

The cylindrical Paul trap has two different settings. The first is using it as an Einzel lens, where the front and back electrodes act as the outer electrodes, while the main cylinder acts as the center electrode. This setting uses no RF on the trap and just allows for a DC ion beam going through. The other option is to utilize the RF on the Paul trap and to actually use it as a trap. This allows for the usage of the Paul trap as a storage device. Since we only need a single molecule within the cryogenic trap, we would like to be able to load ions into the Paul trap, and then using it as a "secondary" ion source, extracting just a few ions at a time for experiments. Additionally it is possible to leak in gas for buffer gas cooling of molecules stored in the cylindrical Paul trap.

Immediately after the Paul trap there is a channel electron multiplier detector (also referred to as a channeltron), which allows us to measure the ion current. This detector has a push/pull feedthrough, allowing it to be moved in and out of the ion beam. This allows us to perform diagnostics on the components of the first half of the detector. Of course if the detector is moved into the ion beam, there will be no ions further down in the setup.

If the first channeltron detector is not in the measurement position, the ions will continue down to another set of Einzel lenses, which focus them into a second octopole, that moves them down to a final set of Einzel lenses, focusing them onto a 2nd channeltron detector. This 2nd detector allows us to measure the ion current that makes it all the way through the ESI part of the experiment. It has to be noted, however, that the 2nd detector sits where the connection to the ion guide will eventually be connected, and as such this is not a permanent installation, but only exists for testing parameters to ensure we are able to get ions to the very end of the ESI source.

3.2 Experiments on the first octopole

The need for getting only single molecular ions in our cryogenic Paul trap poses some very unique challenges for our ESI setup. The dominant one is that in principle ESI sources are usually made to maximize the amount of ions going through. This means that we will need to have a very good understanding of the different parts of the electrospray in order to be able to tailor a protocol for getting single ions to our linear quadrupole trap. For this reason we have spent some time making a characterization of the very first octopole in the experiment. This section contains the results of these measurements. All measurements are performed on rhodamine 6G, since it sprays particularly well.

3.2.1 Measuring the temporal shape of an ion bunch

One of the first characterizations we perform is the temporal shape of an ion bunch leaving the octopole.
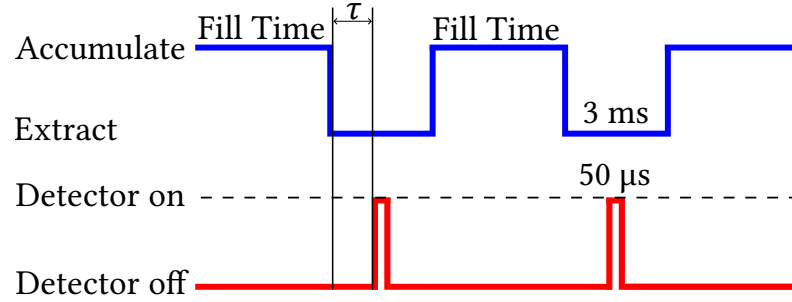
FIGURE 3.4: Illustration of the experimental sequence for measuring the temporal shape of ion bunches leaving the first octopole (figure not to scale). Ions are accumulated (blue) over a preset time (data for 500ms, 30sec, and 1 minute were recorded) and then released. The measurement (red) is turned on for 50μs with a delay τ with respect to the release of the ions. Measurements are repeated 20 times for each value of τ in order to ensure good statistics. By varying τ and recording the number of ions a temporal shape of the ion bunch is recorded.

To get such a measurement we allow ions to accumulate in the octopole for some set amount of time by setting the voltage on the extraction lens to 40V, until the ions are released by lowering the voltage to -10V. After some delay τ we then measure how many ions hit the detector over an interval of 50μs. By repeating this method for several values of τ we are able to get a temporal shape of the ion bunch coming out of the octopole. An illustration of the measurement sequence can be seen on fig. 3.4.

Since it is unclear how narrow the ion bunch is in time, the ion signal is adjsuted such that when the electrospray is in the DC configuration a current of a few 100 ions per second is measured, this ensures the detector will not saturate.

Results from the measurements when the octopole is allowed to accumulate ions for 500ms, 30 seconds and 1 minute can be seen on fig. 3.5. Here three loading times are compared, namely 500ms (green), 30 seconds (blue), and 1 minute (orange). It is seen that the curves for 30 seconds and 1 minute are highly similar, this is likely because they contain very similar amounts of ions as can be seen in CITE LOADING.

The 500ms curve however is considerably slower, both in its rise time and its tail, by approximately a factor of 2. This indicates that the number of ions seems to affect the temperature, with fewer ions leading to colder temperatures. Indeed if we, naively, take the factor 2 difference in time constant to mean that the ions are half as slow, we find that if the ions are loaded for 500ms, they are about a quarter of the temperature of the ions that are loaded over 1 minute or 30 seconds.

It is not surprising to see that a higher number of ions in the octopole lead to higher temperatures. Firstly, the octopole is an RF device, and thus there will always be micromotion, (much like the quadrupole of chapter 2) for any ions that do not lie exactly on the center axis of the octopole. As more and more ions are loaded into the octopole, more of them will find their equilibria further off-axis, where the micromotion is larger, leading to hotter ions.

In addition as the number of ions in the storage device increases, ion-ion collisions become more likely. It is known that such collisions in RF devices will lead to heating of the ion cloud [1, 3].
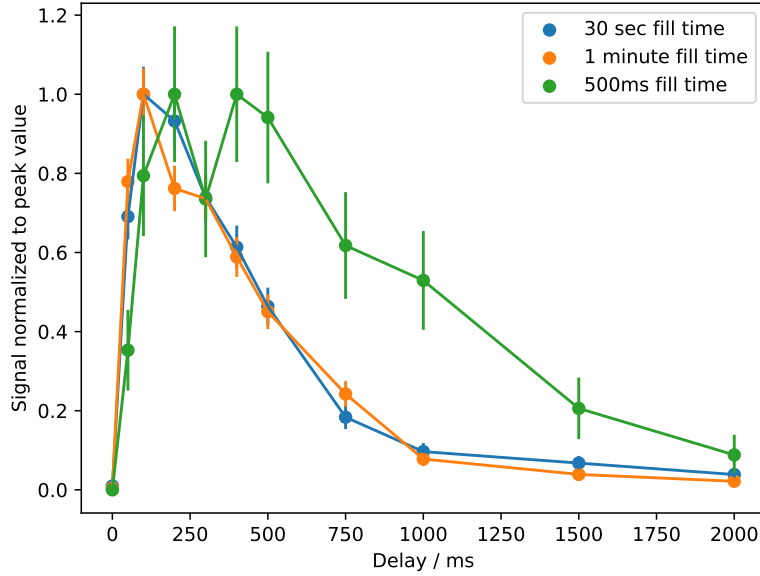
FIGURE 3.5: Plot showing the temporal shape of ion bunches, when the octopole is allowed to fill for 500ms (green), 30 seconds (blue), and 1 minute (orange). Each curve has been normalized to its peak value, in order to allow comparison of the curves. From the measurements it is clear that the majority of ions will arrive during the first second if there are few ions in the octopole (500ms). The width of the pulse is shortened considerably down to approx 500ms if the octopole is allowed to fill. Thus if one wants to be careful of saturating the channeltron detector it is likely best to assume that when an ion bunch is released, all the ions will arrive during 500ms, as this allows some overhead. A feature to note is that the 500ms curve, seems to have a slope that is approx half as steep as the other two curves at the earliest part of the bunch. If one considers the tail we also see that the 500ms curve is approximately a factor two slower here as well. This gives a qualitative indication that loading fewer ions into the octopole, gives a colder distribution of ions.

3.2.2   Measuring the fill time of the octopole

Another characterization that has been performed of the first octopole of the setup is testing how long it takes the octopole to reach the limit of the number of ions it can hold. In order to test this, the octopole is allowed to fill for a variable time τ, after which the ions are released, and the channeltron detector records the total number of ions. By doing this for increasing times we expect to see a behaviour where the number of ions increases linearly in time initially, until eventually space charge effects start to play a role. When these effects come into the picture the loading of ions will progress slower as new ions arriving become able to knock "old" ions out of the octopole, until eventually a steady state is realized. An illustration of the experimental sequence can be seen on fig. 3.6.

All measurements for this experiment were taken at an ion current of approx 300 ions/second, measured at the channeltron detector. The ion current measured at the detector usually varies within 10% due to fluctuations in flow from the electrospray. Thus, any measurements of how long it takes to fill the octopole have to be adjusted
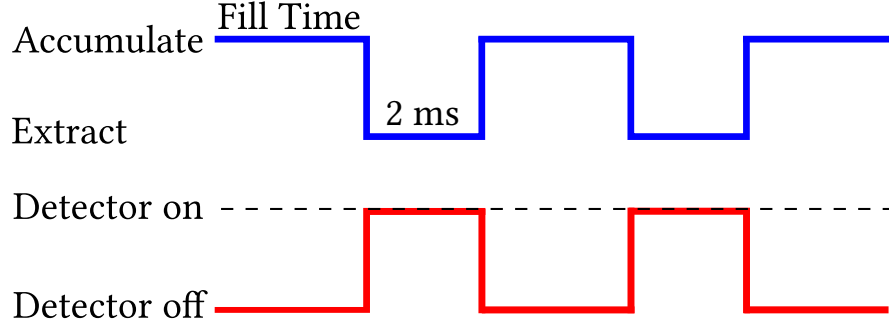
FIGURE 3.6: Illustration (not to scale) of the measurement sequence used to obtain the results of this subsection. The octopole is allowed to fill with ions for variable times. The octopole is allowed to open for 2 ms, which is sufficient to let all the ions leave (see fig. 3.5). During the time when the octopole is open, the channeltron detector is turned on, to count the number of ions. For each fill time this procedure is repeated 20 times..

for the ion flux during the loading phase. This adjustment is done by multiplying the physical loading time by the ratio between the reference of 300 ions/s and the mean of the measured current before and after the experiment giving

$$\tau' = \frac{I_{reference}}{I_{measured}}\tau, \quad I_{measured} = \frac{I_{before} + I_{after}}{2}. \tag{3.1}$$

Results from the experiment with the time-axis adjsuted as described above can be seen on fig. 3.7. From this we can make a very rough estimate of the ion current entering the octopole. The density of ions in an octopole, where space-charge effects are included, can be written CITE MAJIMA

$$n(r) = \frac{144\epsilon_0 V_{RF}^2}{m\Omega^2 r_0^4}\left(\frac{r}{r_0}\right)^4, \tag{3.2}$$

where V_{rf} is the RF voltage of the octopole (170V), m is the mass of the ion (479 amu), Ω is the frequency of the octopole RF voltage ($2\pi \times 2.7\text{MHz}$) and r_0 is half the distance between opposing octopole rods (2.75mm).

In order to get the linear density one has to integrate this in the radial plane. It is of course important to ensure that we integrate out to the right distance from the center axis. Gerlich suggests that the ions can be stored out to $r = 0.8r_0$, by geometric considerations GERLICH. We use this as it is an easy bound to implement. However the cutoff radius of the ion cloud might become more complex to describe when we are in the space-charge dominated regime CITE MAJIMA, as is the case when the octopole is full. We find the number of ions held in the octopole (length of 133mm) to be

$$N = \frac{48\pi\epsilon_0 V_{RF}^2 L}{m\Omega^2 r_0^2}\left(\frac{4}{5}\right)^6 \approx 7.77 \times 10^8. \tag{3.3}$$

Again this number is likely to be lower in reality, but gives a ballpark figure for the number of ions that can be stored in the trap. Assuming the trap is full after 45 seconds of accumulation, we find there is a current of approx. 17×10^6 ions/s entering the octopole while the electrospray is turned on.
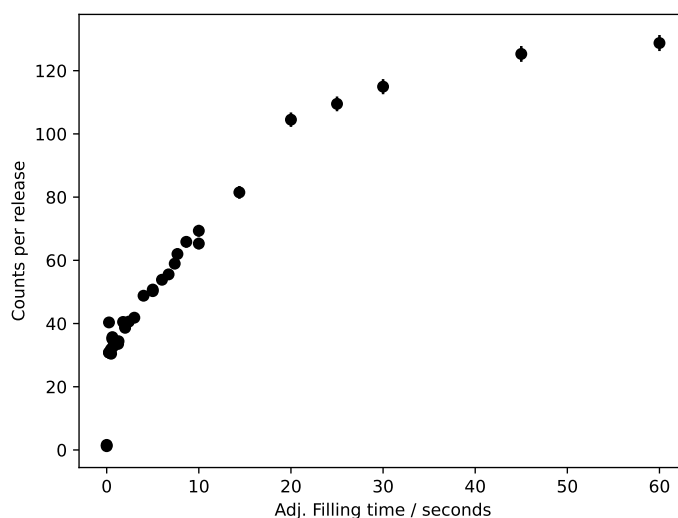
FIGURE 3.7: Results of the measurement of filling time of the octopole. For very low fill times there seems to be a very rapid increase in signal, which then becomes linear until approx. 15 seconds. After this the curve starts tapering off as the number of ions in the detector starts capping out in the mid-late 40s range.

3.2.3   Storage time of the octopole

The final measurement that has been performed on the first octopole aims to determine the period of time, in which ions can be kept in the octopole. Since the the electrospray setup is open to atmosphere, the pumps in the setup have to work hard to ensure low pressure at the end of the setup. If the ions can be stored in the octopole for sufficiently long periods of time, that experiments may be performed using only the ions stored in the octopole, then it is possible to plug the opening of the electrospray, allowing for better vaccuum in the system.

In order to measure the lifetime of ions stored in the octopole, we allow the ions to accumulate in the octopole for 25 seconds after which we turn off the ion current into the octopole, by increasing the voltage on the skimmer to 200V. An illustration of the experimental sequence can be found on fig. 3.8.   Experimental results are seen on fig. 3.9. From the figure it is evident, that there are two timescales at play, when determining the lifetimes of the ions. For the first two minutes there is a rapid loss of ions, which if fitted to an exponential curve leads to a half of 359 ± 249s. After the heavy losses in the first few minutes the curve flattens out considerably. If an exponential decay is fitted to this part of the data a half life of 5243 ± 2782s is obtained. The reason for the large uncertainties in the half lives is that the statistics for the data aren't very good. Especially for the measurements at high storage times, data acquisition times become prohibitve as a single measurement takes an upwards of an hour.

The fact that there are two timescales at play indicates that space-charge effects are important when the octopole is full. A possible explanation for why the ions die off as they do, is that initially the ions are experiencing ion-ion collisions, causing
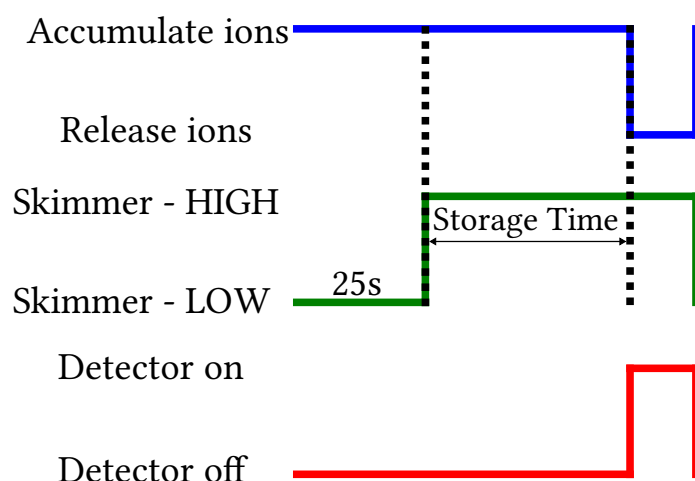
FIGURE 3.8: Illustration of the experimental sequence for measuring lieftime of ions in the octopole. The octopole (blue) is set to its accumulation voltage initially. The skimmer (green) is set to a low voltage of 40V for 25 seconds, allowing ions to enter the octopole. After 25 seconds have passed a voltage of 200V is applied to the skimmer. This blocks ions from entering the octopole. The ions are then kept in the octopole for a time, which is varied for each measurement, after which the ions are released and measured at the detector (red). Measurement is only performed once for the majority of timestamps..

heavy losses on the time-scale of minutes. As more and more ions are lost, the density within the octopole drops to a point, where ion-ion interactions no longer dominate losses in the octopole. At this point the losses will be largely due to ion collisions with the neutral background gas. The measurements indicate that the timescale of this process is on the scale of hours. Thus, it will likely be possible to use the octopole as an ion storage device, allowing for the closing of the electrosapray after an initial loading. Closing off the electrospray to atmosphere is even likely to improve the storage time in the octopole since the long-term storage is determined by collisions with atmospheric air. The lower pressure obtained when the electrospray should lower the rate of collisions, and thus further minimize losses.
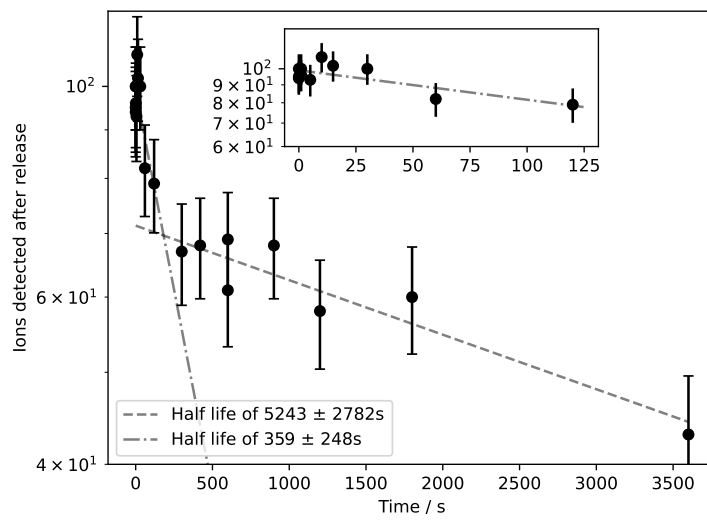
FIGURE 3.9: Measurements of the lifetime of ions in the octopole. There clearly appear to be two timescales. At the short timescale (see inset), the number of ions in the octopole appear to be decaying with a half-life on the order of magnitude of minutes (dashed-dotted line). Conversely for longer timescales the rapid decay is no longer present and instead the population in the trap is decaying on the scale of hours (dahsed line). The cause for the initial rapid loss of population is likely ion-ion collisions within the trap, as the internal dynamics in the trap are initially dominated by space-charge effects. Eventually the ion density becomes sufficiently low to the point where the ions no longer feel one another, and instead losses are dominated by collisions with the background gas..

Cooling

A prerequisite for performing photon recoil spectroscopy, is that the system which is investigated, is cooled to the quantum mechanical ground state of its motion. Cooling of ions in linear Paul traps usually occurs in two stages. First the ion(s) is cooled to approx. 1mK by Doppler cooling, as is described in section 4.1.

When the ion(s) has been cooled to mK tempearture by Doppler cooling, it starts exhibiting quantum mechanical properties. Since the potential in the trap is harmonic, the wavefunction of the ion(s), is that of the harmonic oscillator. To reach the quantum ground state, it is necessary to perorm sideband cooling which takes the ion(s) from whichever $|n\rangle$ state it starts in, and moves it to the state $|0\rangle$ of the harmonic oscillator. This process is described in section 4.2.

Finally there may be some complications to the above cooling processes if we consider two ions with very large charge-to-mass mismatch as explained in section 2.2. Section 4.3

4.1   Doppler cooling

The very first part of cooling two ions down consists of Doppler cooling WINELAND. This method of laser cooling was pioneered by David Wineland and relies on detuning laserlight with respect to an internal transition of the ion, in order to effectively generate a drag force on the ion, cooling it down.

An ion in motion experiences, with a velocity $\boldsymbol{v}$, experiences a Doppler shift of laser light with wave vector $\boldsymbol{k}$ according to

$$\omega_{obs} \approx (1 - \boldsymbol{k} \cdot \boldsymbol{v})\omega_L, \tag{4.1}$$

where ω_{obs} is the frequency seen by the ion, and ω_L is the frequency of the laser in the laboratory frame. Thus if we detune the light of the laser to be below the frequency of an electronic transition in the ion ω, the ion will preferentially absorb photons, when it is propagating against the direction of the light. Due to conservation of momentum, the ion must change its momentum by

$$\Delta \boldsymbol{p} = \hbar \boldsymbol{k}. \tag{4.2}$$

After a short time the ion will decay to the ground state once again, but since the direction of the photon emitted during decay is symmetric, this will, if averaged over multiple emissions, lead to no change in momentum. Thus the momentum of the ion is effectively decreased, since the ion preferentially absorbs photons propagating in the oppsite direction of itself. At low velocities $kv \ll \Gamma$, where Γ is the decay rate of the excited state, one can express this as a drag force (assuming 1D problem to ease notation) KARIN:

$$F_{drag} = -\beta v, \quad \beta = \frac{8\hbar s k^2 \delta / 2\Gamma}{\left(1 + s + (2\delta/\Gamma)^2\right)^2}, \tag{4.3}$$

where β is the drag coefficient, $\delta = \omega_L - \omega$ is the detuning of the laser with respect to the atomic transition, $s = I/I_{sat}$ is the saturation parameter, where I is the intensity of the laser light, and $I_{sat} = \frac{\pi hc}{3\lambda}\Gamma$, with λ being the wavelength of the laser, is the saturation intensity of the transition.

It is important to note, that while the equation above seems to indicate that there is no limit to Doppler cooling, that is far from the case. Indeed since the direction of an emitted photon is random, the ion will perform a random walk in momentum space over time. Thus, there is an intrinsic variation of velocity over time, meaning there is a lower limit to the temperature of the ion (typically referred to as the Doppler temperature or Doppler limit), which is given by

$$T_D = \frac{\hbar\Gamma}{2k_b}, \tag{4.4}$$

which for the case of Ba$^+$ this temperature is approx. 0.5mK.

Of course Doppler cooling only works for very specific ions, that have the proper level-scheme, and is thus not a very good candidate for cooling arbitrary molecular ions. The solution to this problem of not being able to doppler cool molecular ions comes in two parts. Firstly at high temperatures the hot molecular ion will interact with the cooled atomic ions, via the Coulomb interaction. Such interactions will cause the molecular ion to transfer energy to the atomic ion, from which the energy will then be removed by the system via Doppler cooling. This method of cooling is called sympathetic cooling CITE MICHAEL (2000) AND REVIEW by Willitsch In this case we imagine ideally trapping the molecule with a large amount of Ba$^+$ ions to offer the most cooling.

As temperatures drop low enough that the motion truly becomes harmonic, the motion of the ions becomes coupled. As such, the ions will have common motional modes, and any energy extracted from the Ba$^+$ ion is extracted from the mode as a whole, thus cooling the molecular ion as well. This cooling mechanism is only effective if the ions share similar mass-to-charge ratios, however. In the case where the ion motions are nigh uncoupled, as described in section 2.2, further steps must be taken to get the molecular ion to mK temperatures. This is described in section 4.3.

4.2 Sideband Cooling

Unfortunately, Doppler cooling is not sufficient for reaching the motional ground state. In order to do this we employ yet another method of laser cooling, called

sideband cooling cite. When the ions are at the doppler temperature, they will be cold enough that they behave as a quantum mechanical harmonic oscillator, with their wave function being a thermal distribution over the Fock states $|n\rangle$. By coupling the state $|g, n\rangle$ to the state $|e, n-1\rangle$ where (e, g) denotes the excited and ground states of the atom, we are able to remove one quanta of energy from the motion under an excitation of the electronic state. Since the electronic state predominantly decays to the same n, this allows us to cool the ion's motion by moving down the "ladder" seen on fig. 4.1

We initially consider a single atomic ion in the Paul trap, and neglect the radial modes of motion in order to ease notation. The Hamiltonian can be written as

$$\hat{H}_0 = \hbar\omega_z(\hat{n} + 1/2) + \hat{H}_a, \tag{4.5}$$

where $\hat{n}$ is the Fock state number operator, and $\hat{H}_a$ is the Hamiltonian for the atomic system. If a laser field is turned on at some detuning $\delta = \omega_L - \omega$ with respect to the electronic transition of the ion, the interaction with the laser in the interaction picture is described by:

$$H_I = \frac{\hbar\Omega_0}{2}\hat{\sigma}_+\left(e^{ik_z\hat{z}_I}e^{-i\delta t}\right) + h.c., \tag{4.6}$$

where $\hat{\sigma}_+ = |e\rangle\langle g|$ is the excitation operator responsible for exciting the electronic state of the ion, and $\Omega_0 = \frac{eE_0}{\hbar}\langle g|\hat{\epsilon} \cdot \hat{z}|e\rangle$ is the Rabi frequency of the transition, being driven by an electric field of amplitude E_0, and direction $\hat{\epsilon}$. Note that the rotating wave approximation has been applied to the expression above, keeping only slowly rotating terms.

We may express $\hat{z}_I$ in terms of the ladder operators yielding

$$\hat{z}_I = \sqrt{\frac{\hbar}{2m\omega_z}}(\hat{a}e^{-i\omega_z t} + \hat{a}^\dagger e^{i\omega_z t}) \tag{4.7}$$

Before inserting this expression back into eq. (4.6), it will be useful to first define the Lamb-Dicke parameter

$$\eta = k_z\sqrt{\frac{\hbar}{2m\omega_z}}, \tag{4.8}$$

which in the so-called Lamb-Dicke regime, where $\eta\sqrt{\langle n \rangle + 1} \ll 1$ EMILIE allows us to write

$$H_I = \frac{\hbar\Omega_0}{2}\hat{\sigma}_+\left[e^{-i\delta t} + i\eta\left(\hat{a}^\dagger e^{i(\omega_z - \delta)t} + \hat{a}e^{-i(\omega_z + \delta)t}\right)\right] + h.c. \tag{4.9}$$

Here the first term is resonant when $\delta = 0$ and corresponds to the laser being resonant with the atomic transition, driving it with no change in motional quantum number. The second term is resonant when the laser is blue detuned by $\delta = \omega_z$, and increases the motional quantum number while exciting the system, thus heating the system, corresponding to walking up the ladder of fig. 4.1. Finally the third term is resonant when $\delta = -\omega_z$, and removes a phonon at by performing an electronic excitation. Repeatedly performing this process will eventually cool the ion to the ground state, as seen on fig. 4.1.

If we instead consider two ions, the picture changes ever so slightly. In the case where only one of the ions interacts with the laser light, as would be the case for
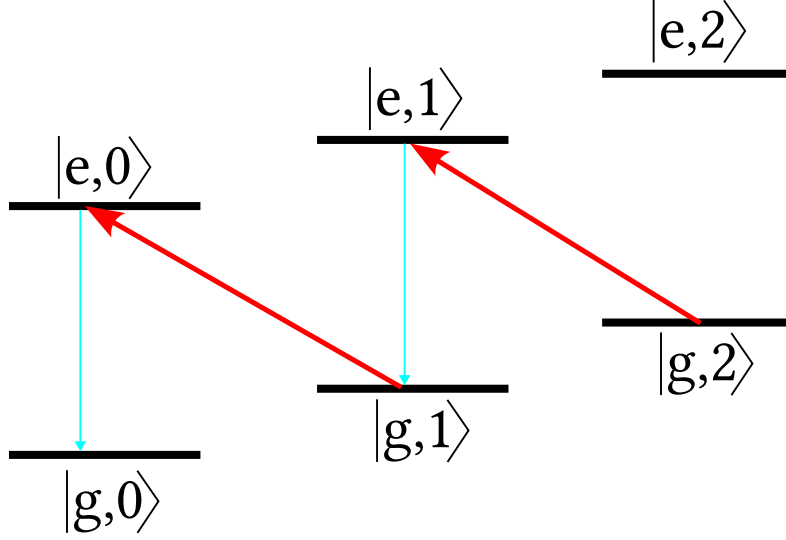
FIGURE 4.1: Illustration of the concept behind sideband laser cooling. The laser (red) is detuned with respect to the electronic transition, by exactly ω_z. Thus transitions are driven at the cost of a phonon. The atom is most likely to decay to the same Fock state, effectively causing it to lose phonons, as several excitations occur. This makes the ion "climb down the ladder" until it reaches the quantum ground state..

Ba^+ cotrapped with a molecule, we simply have to include the mode structure when writing out $\hat{z}_1$. In the case of two ions with in-phase and out-of-phase frequencies of ω_i, ω_o, the motional state of the system is described by the product space $|n_i, n_o\rangle$. Where the subscript (i/o) denotes the in-phase and out-of-phase mode respectively. The position operator for the barium ion in this system can be expressed as

$$\hat{z}_1 = \sqrt{\frac{\hbar}{2m_1}} \left(\alpha_{i,1} \frac{a_i + a_i^\dagger}{\sqrt{\omega_i}} + \alpha_{o,1} \frac{a_o + a_o^\dagger}{\sqrt{\omega_o}} \right), \tag{4.10}$$

where $\alpha_{i/o,1}$ is the participation of the atomic ion in the motion of the mode, as calculated in section 2.2. This operator may be inserted in the place of z_I (remembering to switch to the interaction picture) in equation eq. (4.6). Following an identical derivation we see that sideband cooling is still possible for all modes, provided that $\alpha_{i/o}$ does not get so small, that the coupling becomes too weak.

This clearly poses a problem for systems where the mass-to-charge ratios of the two ions differ considerably, as $\alpha_{i,1} \ll \frac{1}{\sqrt{2}}$ for such systems. Effectively making cooling of the in-phase motion impossible.

4.3   Coupling of motional modes to enhance cooling

As mentioned in both section 4.1 and section 4.2, laser cooling becomes very difficult once the charge-to-mass ratios of the two differ considerably. The reason for this is relatively easy to understand. Since the laser cooling only interacts with the atomic ion, this is the only ion whose motion is cooled through the interaction with the light. In the case where the ions have similar charge-to-mass ratios however,
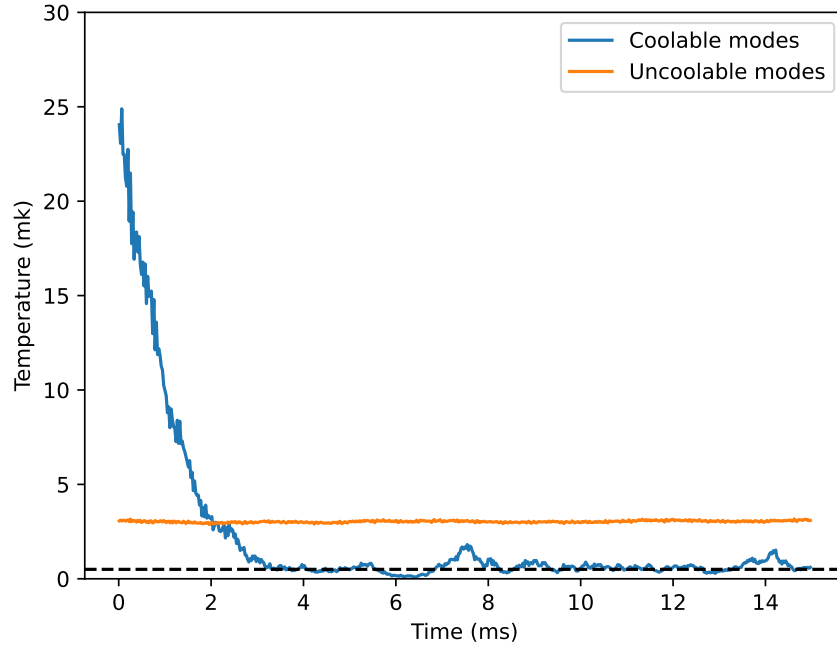
FIGURE 4.2: Simulation of Doppler cooling of a two/ion system, containing of a Ba^+ ion, and a polyporphyrin. Two curves are plotted, corresponding to the tempearture of the modes with high (blue), and low (orange) participation from the Ba^+ ion. Clearly only the modes with a high participation are cooled by the Doppler cooling.

their motions are so strongly coupled, that any cooling of the atomic ion, will cool the molecular ion as well. As the ratios start to differ the motions quickly become uncoupled, and thus the cooling of the atom, no longer affects the molecule in any appreciative way. This is clearly seen on fig. 4.2, which shows the temperature of Ba^+ ion, cotrapped with a polyporphyrine ($m_2 = 9000$ amu, $q_2 = 24e$). The blue curve shows the temperature of the motional modes, that have a large contribution from the atom. Clearly these modes are effectively cooled. In stark contrast we have the orange curve, which displays the temperature of all the modes that have low contribution from the atom, whose temperature remains effectively unchanged.

In fact, this problem reaches further than simply cooling. For example, it is the molecular ion we wish to investigate with photon recoil spectroscopy (PRS). However the momentum kick gained from absorption on the molecule, will predominantly excite the motional modes with high participation from the molecule. Unfortunately the readout method for PRS is very similar to the side-band pulses described in section 4.2, and thus for the same reasons, readout becomes impossible when the coupling grows too weak, since these modes have very small participation from the atomic ion, on which readout is performed.

The solution to this problem is to find some way to couple the two modes, allowing for the transfer energy from one to the other. Curiously enough the need for coupling such modes was present in Penning traps many years ago, in order to cool the so-called magnetron mode of such a trap [2, 4]. For the Pennin trap the

solution found was to add another quadrupole field, oscillating at the frequency difference between the two modes to be coupled, such a solution also works for the case of the Paul trap as has been demonstrated very recently CITE REFEREE.

It is easiest to understand the coupling that occurs, when we consider the quantum mechanical case. Suppose we introduce some additional potential (by modulating a slight additional voltage on the endcap electrodes)

$$V'(z_1, z_2, t) = \frac{\kappa V_0}{z_0^2}(q_1 z_1^2 + q_2 z_2^2)\cos\left([\omega_i - \omega_o]t\right), \tag{4.11}$$

where V_0 is the additional voltage put onto the endcap electrodes. We note that V_0 is kept small with respect to V_{DC}, such that the eigenmodes of the system are not considerably changed.

If we perform a Taylor expansion to second order around the equilibrium (at $V_0 = 0$) positions is performed similarly to section 2.2, we may write (neglecting the offest term)

$$V'(\delta z_1, \delta z_2, t) \approx \frac{\partial V'}{\partial z_1}\bigg|_{eq}\delta z_1 + \frac{\partial V'}{\partial z_2}\bigg|_{eq}\delta z_2 + \frac{1}{2}\frac{\partial^2 V'}{\partial z_1^2}\bigg|_{eq}\delta z_1^2$$
$$+ \frac{1}{2}\frac{\partial^2 V'}{\partial z_2^2}\bigg|_{eq}\delta z_2^2 + \frac{\partial^2 V'}{\partial z_1 \partial z_2}\bigg|_{eq}\delta z_1 \delta z_2. \tag{4.12}$$

For now, we only wish to consider the coupling of the modes, and thus neglect the first-order terms. Clearly these terms cannot couple the modes as $\delta \hat{z}_j \propto (\alpha_{j,o}\hat{a}_o + \alpha_{j,i}\hat{a}_i) + h.c.$ is not sufficient to transfer energy from one mode to another. If we instead consider solely the 2nd. order terms we find

$$\hat{V}'^{(2)} = \frac{\hbar \kappa V_0}{2z_0^2}\cos\left([\omega_i - \omega_o]t\right)\bigg(q_1\big(\frac{\alpha_{1,i}(\hat{a}_i + \hat{a}_i^\dagger)}{\sqrt{m_1\omega_i}} + \frac{\alpha_{1,o}(\hat{a}_o + \hat{a}_o^\dagger)}{\sqrt{m_1\omega_o}}\big)^2$$
$$+ q_2\big(\frac{\alpha_{2,i}(\hat{a}_i + \hat{a}_i^\dagger)}{\sqrt{m_2\omega_i}} + \frac{\alpha_{2,o}(\hat{a}_o + \hat{a}_o^\dagger)}{\sqrt{m_2\omega_o}}\big)^2\bigg). \tag{4.13}$$

If the cosine is expanded using Euler's formula, and we move to the interaction picture, keeping only the non-rotating terms, we may massage the expression and eventually arrive at

$$\hat{V}_I'^{(2)} = \frac{\hbar \kappa V_0 \alpha_{1,o}\alpha_{1,i}}{4z_0^2\sqrt{\omega_i\omega_o}}\big(\frac{q_1}{m_1} - \frac{q_2}{m_2}\big)(\hat{a}_o^\dagger \hat{a}_i + h.c.) \tag{4.14}$$

Photon Recoil Spectroscopy (WHERE SHOULD THIS GO?)

Future Work

In the following, I will outline the topics I will work on in the final part of my PhD
…

Bibliography

[1] R. Blümel et al. 'Chaos and order of laser-cooled ions in a Paul trap'. In: *Phys. Rev. A* 40 (2 July 1989), pp. 808–823. DOI: 10.1103/PhysRevA.40.808. URL: https://link.aps.org/doi/10.1103/PhysRevA.40.808.

[2] B. M. Garraway F. Crimin and J. Verdú. 'The quantum theory of the Penning trap'. In: *Journal of Modern Optics* 65.4 (2018), pp. 427–440. DOI: 10.1080/09500340.2017.1393570. eprint: https://doi.org/10.1080/09500340.2017.1393570. URL: https://doi.org/10.1080/09500340.2017.1393570.

[3] L. Hornekær and M. Drewsen. 'Formation process of large ion Coulomb crystals in linear Paul traps'. In: *Phys. Rev. A* 66 (1 July 2002), p. 013412. DOI: 10.1103/PhysRevA.66.013412. URL: https://link.aps.org/doi/10.1103/PhysRevA.66.013412.

[4] Robert S. Van Dyck, Paul B. Schwinberg and Hans G. Dehmelt. 'New high-precision comparison of electron and positron g factors'. In: *Phys. Rev. Lett.* 59 (1 July 1987), pp. 26–29. DOI: 10.1103/PhysRevLett.59.26. URL: https://link.aps.org/doi/10.1103/PhysRevLett.59.26.